remote sensing

MDPI

Article

Performance Assessment of IMERG V07 Versus V06 for Precipitation Estimation in the Parnaíba River Basin

Flávia Ferreira Batista [1,*], Daniele Tôrres Rodrigues [2,3], Cláudio Moises Santos e Silva [2], Lara de Melo Barbosa Andrade [2], Pedro Rodrigues Mutti [2], Miguel Potes [4] and Maria João Costa [4]

[1] Federal Institute of Espírito Santo (IFES), Presidente Kennedy 29350-000, ES, Brazil
[2] Department of Atmospheric and Climate Sciences, Federal University of Rio Grande do Norte (UFRN), Natal 59078-970, RN, Brazil; mspdany@ufpi.edu.br (D.T.R.); claudio.silva@ufrn.br (C.M.S.e.S.); lara.andrade@ufrn.br (L.d.M.B.A.); pedro.mutti@ufrn.br (P.R.M.)
[3] Department of Statistics, Federal University of Piauí (UFPI), Teresina 64049-550, PI, Brazil
[4] Center for Sci-Tech Research in Earth System and Energy—CREATE, Department of Physics, Universidade de Évora, 7000-671 Évora, Portugal; mpotes@uevora.pt (M.P.); mjcosta@uevora.pt (M.J.C.)
* Correspondence: flavia.batista@ifes.edu.br

Highlights

What are the main findings?

- IMERG V07 reduced systematic errors compared to V06, with lower bias and random errors across most of the basin, while high Rbias values (>70%) persisted in the northeastern highlands due to orographic–convective interactions. Detection capacity also improved, with false alarms reduced by ~5% and KGE increasing by ~11%.
- Cluster-based analysis revealed that V07 better represented seasonal precipitation variability, correcting overestimation in wet periods and underestimation in semi-arid regions.

What is the implication of the main finding?

- These improvements enhance the reliability of IMERG V07 for hydrological and climate applications in tropical basins with strong seasonal variability.
- Persistent errors in mountainous and transitional areas highlight the need for regionalized bias corrections tailored to local climatic and topographic conditions.

Abstract

Accurate satellite-based precipitation estimates are crucial for climate studies and water resource management, particularly in regions with sparse meteorological station coverage. This study evaluates the improvements of the Integrated Multi-satellite Retrievals for GPM (IMERG) Final Run version 07 (V07) relative to the previous version (V06). The evaluation employed gridded data from the Brazilian Daily Weather Gridded Data (BR-DWGD) product and ground observations from 58 rain gauges distributed across the Parnaíba River Basin in Northeast Brazil. The analysis comprised three main stages: (i) an intercomparison between BR-DWGD gridded data and rain gauge records using correlation, bias, and Root Mean Square Error (RMSE) metrics; (ii) a comparative assessment of the IMERG Final V06 and V07 products, evaluated with statistical metrics (correlation, bias, and RMSE) and complemented by performance indicators including the Kling-Gupta Efficiency (KGE), Probability of Detection (POD), and False Alarm Ratio (FAR); and (iii) the application of cluster analysis to identify homogeneous regions and characterize seasonal rainfall variations across the basin. The results show that the IMERG Final V07 product provides notable improvements, with lower bias, reduced RMSE, and greater accuracy in representing the spatial distribution of precipitation, particularly in the central and southern regions of the basin, which feature complex topography. IMERG V07 also demonstrated higher

check for updates

Academic Editor: Yuriy Kuleshov

Received: 9 September 2025
Revised: 24 October 2025
Accepted: 28 October 2025
Published: 31 October 2025

Citation: Batista, F.F.; Rodrigues, D.T.; Santos e Silva, C.M.; Andrade, L.d.M.B.; Mutti, P.R.; Potes, M.; Costa, M.J. Performance Assessment of IMERG V07 Versus V06 for Precipitation Estimation in the Parnaíba River Basin. *Remote Sens.* **2025**, *17*, 3613. https://doi.org/10.3390/rs17213613

consistency, with reduced random errors and improved seasonal performance, reflected in higher POD and lower FAR values during the rainy season. The cluster analysis identified four homogeneous regions, within which V07 more effectively captured seasonal rainfall patterns influenced by systems such as the Intertropical Convergence Zone (ITCZ) and Amazonian moisture advection. These findings highlight the potential of the IMERG Final V07 product to enhance precipitation estimation across diverse climatic and topographic settings, supporting applications in hydrological modeling and extreme-event monitoring.

Keywords: IMERG; satellite rainfall evaluation; cluster analysis; Parnaíba River Basin

1. Introduction

Accurate and reliable precipitation estimates are fundamental to hydrological analyses, water resource management, and disaster early warning systems. This importance is further amplified in the context of a changing climate, where the intensification and increased frequency of extreme weather events, such as droughts and floods, pose significant threats to vulnerable regions. In South America, and particularly in Brazil, these changes heighten the risk of large-scale droughts and severe flooding, directly impacting water security and ecosystem stability [1]. The watersheds in northeastern Brazil (NEB) exemplify this vulnerability, as demonstrated by Rudorff et al. [2]; climate change has increased the probability of flooding events in the Parnaíba River by approximately 30%. The authors highlight the evolving complexity of hydrometeorological and anthropogenic processes affecting flood risks, emphasizing the necessity for continuous risk assessment and the implementation of suitable mitigation strategies. The complex nature of these impact studies in the region is further corroborated by other studies [3,4].

In 2023, the IMERG V07 was released, introducing advancements in bias correction and estimation accuracy, especially under complex conditions such as mountainous terrains, frozen surfaces, and coastal regions [5]. Subsequent validation studies have demonstrated these improvements across diverse global contexts. Evaluations in China showed that V07 exhibited reduced RMSE and better consistency with ground data compared to V06, although challenges in capturing intense and light precipitation events persisted [6]. When applied to flood modeling in a Chinese river basin, V07 showed a tendency to overestimate flood peaks due to precipitation overestimation; however, its performance saw substantial improvements after bias correction [7]. A key advancement in V07 addressed the spatial misplacement of rainfall events over oceans, an issue identified in the previous version, which resulted in improved oceanic rainfall statistics [8]. Further validation in Indonesia confirmed V07's improved capability in observing diurnal precipitation patterns compared to V06, though limitations in representing daytime rainfall intensity remained [9].

Recent comparative studies indicate that IMERG V07 outperforms other satellite precipitation products, such as the Global Satellite Mapping of Precipitation (GSMaP) and Precipitation Estimation from Remotely Sensed Information using Artificial Neural Networks (PERSIANN), across various temporal and spatial scales, particularly during intense rainfall events. For instance, Wang et al. [10] conducted a comprehensive analysis highlighting significant improvements of V07 compared to GSMaP, and Watters et al. [8] observed IMERG V07 to be more reliable than PERSIANN, especially in areas of complex topography.

In the South American context, [11] performed a comparative assessment between IMERG versions V06 and V07, identifying critical discrepancies in oceanic and continental areas. Focusing specifically on Brazil, these authors segmented the country into five distinct rainfall regimes (R1–R5), demonstrating that V07 significantly reduced RMSE and

improved categorical metrics in areas dominated by cold-top convective clouds. However, precipitation estimates remained underestimated in regions influenced by warm-top clouds, particularly in Brazil's semi-arid region.

While these national-scale studies provide valuable insights, they mask critical heterogeneities at the basin level, where topography and climatic gradients create a complex and spatially varied rainfall regime. This study addresses this specific gap by focusing on the Parnaíba River Basin. The strategic importance of this basin is threefold: (1) it is one of the largest and most diverse hydroclimatic systems in NE Brazil, encompassing steep gradients from humid headwaters to semi-arid lowlands; (2) it is a vital water resource for millions of people and a key part of the MATOPIBA agricultural frontier, making accurate rainfall data crucial for water security and economic planning; and (3) its complex mix of rainfall regimes makes it an ideal natural laboratory to test IMERG's performance under challenging and diverse conditions, directly addressing the calibration gaps highlighted by [11] for regions like Northeastern Brazil.

At the global level, recent works such as Rozante & Rozante [11] and Guo et al. [6] have emphasized the relevance of regional validation efforts for IMERG V07, as they provide critical feedback for refining retrieval algorithms and improving product calibration. The present study contributes to this ongoing effort by extending V07 validation to northeastern Brazil—a region characterized by complex rainfall dynamics and limited gauge density—thus adding a novel regional perspective to the global understanding of IMERG performance. Shimizu et al. [12] emphasize the necessity of understanding the impacts of climate change in Amazonian and NEB river basins in Brazil, where precipitation patterns and underlying physical mechanisms exhibit notably high variability.

These studies underscore the importance of continuous evaluation of satellite precipitation products to monitor climate dynamics. The enhancements introduced by IMERG V07 represent a significant advancement in the detection of climate variability. Nevertheless, as highlighted by Rozante et al. [11], critical gaps remain, especially regarding regional calibration in regions such as northeastern Brazil, where seasonal variability and sparse rain gauge coverage may compromise rainfall estimate accuracy, thereby influencing public policy decisions and climate adaptation strategies.

Given the above considerations, the present study aims to conduct a comparative analysis of the IMERG V06 and V07 products over the Parnaíba River Basin, part of which overlaps with the MATOPIBA region—an acronym formed from the initials of the states Maranhão (MA), Tocantins (TO), Piauí (PI), and Bahia (BA)—an expanding agricultural frontier in Northeast Brazil. In addition to contributing to the validation of IMERG V07 in an area with limited rain gauge coverage, this work seeks to investigate how high-resolution Brazilian Daily Weather Gridded Data (BR-DWGD), combined with cluster analysis techniques, can improve the understanding of seasonal and regional rainfall variability. It is expected that the outcomes of this study will feed the development of hydrometeorological disaster adaptation and mitigation policies and strengthen water resource management in tropical regions affected by extreme weather events.

2. Materials and Methods

2.1. Study Area

The study area is the Parnaíba River Basin (PRB), located in Northeastern Brazil. Covering approximately 333,920 km^2, the basin lies between the coordinates 2°21′S to 11°06′S latitude and 47°21′W to 39°44′W longitude, with a surface water availability of about 379 m^3/s, making it the second most important basin in NEB in terms of hydrology [13] (Figure 1). The basin's primary watercourse, the Parnaíba River, originates in the Chapada das Mangabeiras plateau, at the boundary of the states of Piauí, Maranhão, Bahia, and

Tocantins, flowing northward and discharging into the Parnaíba Delta, the largest open-sea delta in the Americas [14].

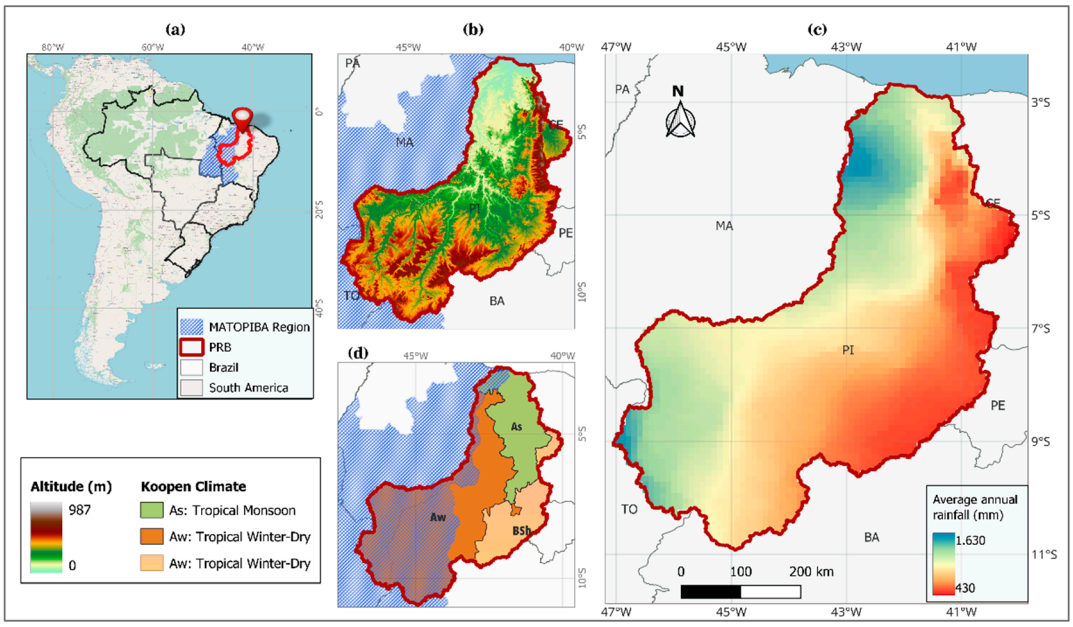

Figure 1. Geographic location (**a**), altitude (**b**), average annual rainfall (AAR, 2001–2020, BR-DWGD) (**c**), and Köppen climate classification (**d**) of the Parnaíba River Basin (PRB), Brazil.

The PRB encompasses areas with different climate types: tropical with a dry winter season (Aw), hot semi-arid (BSh), and tropical with a dry summer season (As). These climates are influenced by rainfall patterns and the availability of water resources in the region [15]. Rainfall patterns are particularly critical for the MATOPIBA region, a major soybean production area encompassing portions of the states of Maranhão, Tocantins, Piauí, and Bahia. Rainfall variability is influenced by phenomena such as the El Niño–Southern Oscillation (ENSO) and the Tropical Atlantic thermal gradient [16]. The rainy season occurs primarily from February to August in the northern basin and from September to January in the southwestern area [17] (Figure 1).

The mean annual temperature in the PRB is approximately 27 °C, with predominant vegetation types including Caatinga in semi-arid areas and Cerrado vegetation covering most of the basin [18]. The basin features diverse terrain, ranging from flat lowlands to mountainous areas, with altitudes varying from sea level up to approximately 900 m [19]. According to the Brazilian Institute of Geography and Statistics (IBGE), the region's total population is around 4.15 million inhabitants, with approximately 35% residing in rural areas [13]. Precipitation shows pronounced seasonal variability, with a mean annual total of approximately 1064 mm. The rainy season occurs from December to April, with monthly averages near 150 mm. The dry season extends from June to November, with rainfall dropping to around 22 mm per month, while May acts as a transitional month [20].

2.2. Data Sources

The datasets used in this study include three primary sources: (i) rainfall records from conventional rain gauges, (ii) precipitation estimates from versions V06 and V07 of the IMERG Final product, and (iii) gridded precipitation data provided by Xavier et al. [21]. The analysis period extended from January 2001 to December 2020.

a. Conventional Rain Gauge Data

Daily rainfall data were obtained from 58 rain gauges distributed throughout the PRB, sourced from monitoring networks such as the National Institute of Meteorology (INMET) and the National Water Agency (ANA). Only stations with less than 30% missing data in their time series were selected, corresponding to occasional missing days distributed throughout the record rather than entire missing years. Days without records were excluded from the analysis.

Outlier detection followed the quality-control procedure proposed by Xavier et al. [21,22]. Daily values were visually inspected and compared with historical climatology and neighboring stations to identify anomalous or physically implausible records. Outliers were removed when they exceeded regional precipitation limits (e.g., >450 mm day^{-1}) or were negative, ensuring internal consistency without altering valid observations. No correction or gap-filling methods were applied, thereby preserving the integrity of the original observed data.

The locations of the rain gauges are indicated by blue points in Figure 2c. The gauges are distributed across the main Köppen climate zones of the basin, with approximately 66% located in Aw (Tropical Winter-Dry), 24% in As (Tropical Monsoon), and 10% in BSh (Tropical Semi-Arid) areas. These proportions are consistent with the real extent of each climatic zone (Aw ≈ 67%, As ≈ 14%, and BSh ≈ 13%), confirming the adequate spatial representativeness of the rain gauge network.

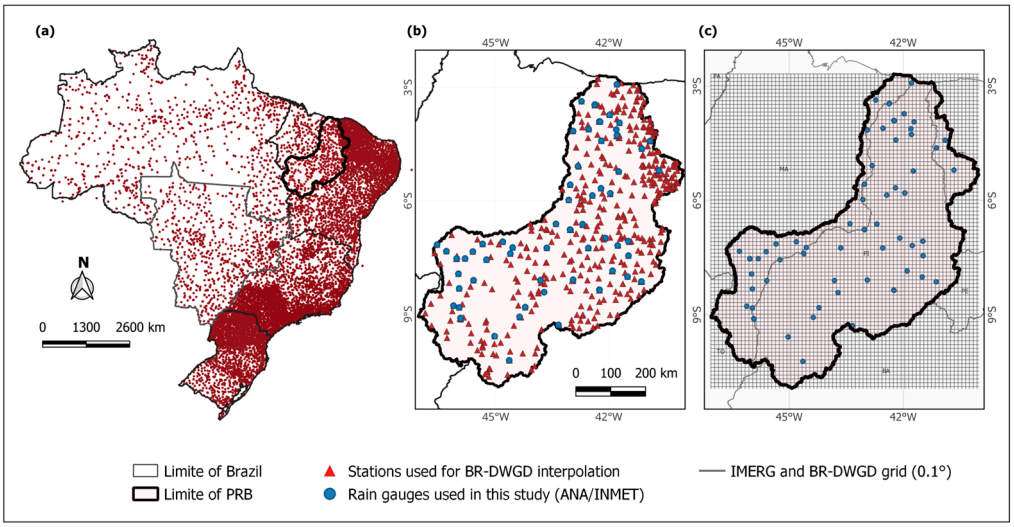

Figure 2. Spatial distribution of the rain gauge networks and gridded datasets used in this study. (**a**) BR-DWGD stations across Brazil [22]; (**b**) overlap between BR-DWGD network and rain gauges used in this study; (**c**) IMERG and BR-DWGD 0.1° grid over the Parnaíba River Basin (PRB).

b. Gridded Interpolated Data (BR-DWGD)

High-resolution precipitation data from the Brazilian Daily Weather Gridded Data (BR-DWGD) were used, arranged in a regular horizontal grid with 0.1° × 0.1° spatial resolution. This dataset is derived from measurements obtained through an extensive network comprising 1252 meteorological stations, including 642 conventional and 610 automatic stations, in addition to 11,473 rain gauges distributed throughout Brazil (Figure 2a) [21,22].

Figure 2 illustrates the spatial distribution of the datasets used: (a) BR-DWGD stations across Brazil; (b) overlap between the BR-DWGD network and the 58 rain gauges used in this study; and (c) IMERG and BR-DWGD 0.1° grid covering the PRB. The BR-DWGD network shows greater station density in the central and northeastern regions of the basin, reflecting the stronger observational coverage in these sectors, while the southwestern

portion has comparatively fewer stations due to the spatial distribution of the national monitoring network.

Precipitation fields in this dataset are interpolated using the Inverse Distance Weighting (IDW) method, which showed superior statistical performance in a comprehensive cross-validation analysis detailed by Xavier et al. [22]. The authors compared six interpolation techniques (IDW, ADW, kriging, spline, natural neighbor, and arithmetic mean) and found that IDW provided the lowest bias and RMSE for precipitation, while ADW performed better for other variables. Each grid point is estimated from the five nearest gauges, with weights inversely proportional to the distance between the target and observation points. In addition, the authors applied a refinement for precipitation, averaging multiple sub-grid interpolations (0.05° spacing) to better represent rainfall spatial variability.

These data were selected to capture spatial variability and fill gaps, ensuring temporal and spatial compatibility with IMERG and rain gauge data. Available in NetCDF format, the daily data have the same resolution as the IMERG Multi-satellite retrievals [23]. The BR-DWGD is continuously updated and freely available at https://sites.google.com/site/alexandrecandidoxavierufes/brazilian-daily-weather-gridded-data (accessed on 6 June 2025).

Over the Parnaíba River Basin (PRB), approximately 490 stations contributed to the interpolation performed by Xavier et al. [21], with the highest network density observed in the central and northeastern portions of the basin and sparser coverage in the southwest. In this study, 58 conventional rain gauges from ANA and INMET networks were used, corresponding to stations with continuous operation between 2001 and 2020 and less than 30% of missing data. Although part of these gauges may overlap with those used in the BR-DWGD interpolation, this subset represents a much smaller and temporally restricted sample of the broader set of stations used by Xavier et al. [21].

The BR-DWGD dataset is extensively used in studies focused on climatic variability, changes in precipitation patterns, satellite precipitation product validation, extreme event monitoring, and hydrological analyses [24–27]. In this study, BR-DWGD data were first evaluated against local rain gauge measurements to verify interpolation accuracy and then employed as a reference to assess the performance of IMERG precipitation estimates across the entire spatial extent of the Parnaíba Basin, rather than just at specific points.

c. Satellite Precipitation Products (SPPs)

The IMERG is a NASA dataset derived from multiple satellites under the Global Precipitation Measurement (GPM) program. It provides precipitation estimates with a high spatial resolution of 0.1° and a temporal sampling of 30 min. In 2023, version V07 was released, bringing significant improvements over V06, including updated input algorithms, corrections for spatial displacement errors, improved passive microwave intercalibration, automated quality control for infrared data, and increased precipitation rate limits up to 200 mm/h [5]. These improvements have led to enhanced accuracy and reliability of precipitation estimates, benefiting research and climate monitoring. Moreover, the final version of IMERG V07 offers reduced latency, ensuring more consistent near-real-time data availability [5]

Precipitation data from GPM IMERG Final versions V06 and the reprocessed V07B V07 were obtained from the Final Run Daily product provided by NASA, which represents the official daily accumulation derived from the half-hourly IMERG estimates. This dataset, with 0.1° spatial resolution. The IMERG Final Daily products are available through NASA platforms such as the NASA Data and Information Services Center (https://disc.gsfc.nasa.gov/; accessed on 1 May 2024) and Giovanni (https://giovanni.gsfc.nasa.gov/; accessed on 1 May 2024), enabling comparative analyses of precipitation estimates within a 2765-point spatial grid covering the Parnaíba River Basin (Figure 2).

Although some INMET and ANA stations used in the BR-DWGD dataset may also contribute to the GPCC analysis employed for IMERG Final Run calibration, the GPCC adjustment is applied at a monthly timescale, while the present study evaluates daily precipitation estimates. Consequently, the analysis can be regarded as regionally and temporally independent, reflecting the true performance of IMERG products over the Parnaíba River Basin.

2.3. Methods

2.3.1. Evaluation Framework

The evaluation framework adopted in this study was designed to assess the performance of the IMERG precipitation estimates (Final Run V06 and V07) across multiple spatial and temporal scales, following a two-step hierarchical approach.

Step 1—Point-scale evaluation: The first stage validated BR-DWGD interpolated precipitation data against daily observations from 58 rain gauges distributed across the Parnaíba River Basin (PRB), verifying its reliability as a reference product for subsequent satellite evaluation.
Step 2—Gridded-scale evaluation: After confirming the consistency of BR-DWGD data with ground observations, IMERG products were compared against BR-DWGD estimates over a regular $0.1^\circ \times 0.1^\circ$ grid (2765 points), enabling a spatially continuous assessment of IMERG performance across the entire basin domain.

Temporal dimension:

Analyses were carried out at the daily scale and aggregated by season, distinguishing between wet (DJF–MAM) and dry (JJA–SON) periods, according to the World Meteorological Organization (WMO) standard classification: DJF (December–February), MAM (March–May), JJA (June–August), and SON (September–November).

Regional (cluster-based) analysis:

To capture the spatial heterogeneity of precipitation patterns within the PRB, a regionalization procedure was applied using BR-DWGD and IMERG data. Homogeneous regions (clusters) were delineated to compare IMERG V06 and V07 performance across distinct climatic and geographic contexts. The detailed clustering procedure is described in Section 2.3.2. Non-parametric statistical tests were used to determine whether differences in performance among clusters and between versions were significant (Section 2.3.3).

This hierarchical framework integrates point-scale validation, basin-wide assessment, and seasonal–regional analyses to provide a comprehensive evaluation of IMERG performance and to identify spatial patterns and potential sources of uncertainty in satellite-based precipitation estimates.

2.3.2. Cluster Analysis

The clustering analysis was performed using gridded BR-DWGD precipitation data at $0.1^\circ \times 0.1^\circ$ spatial resolution for the 20-year period (2001–2020). For each grid point, monthly accumulated precipitation was averaged across the years to produce climatological monthly means, annual totals, and mean annual precipitation. This procedure preserves the spatial and temporal characteristics of the rainfall regime, enabling the identification of homogeneous regions that represent persistent climatic patterns rather than artifacts of temporal averaging.

The objective of the analysis was to delineate homogeneous rainfall regions within the Parnaíba River Basin (PRB) by grouping grid points with similar precipitation behavior while maximizing contrast between clusters. The optimal clustering configuration was determined using BR-DWGD data, which served as the reference dataset for defining both

the grouping method and the number of clusters. Once this configuration was established, the same methodology and cluster structure were applied to the IMERG V06 and V07 datasets, ensuring methodological consistency and allowing direct spatial comparison between satellite-derived and interpolated precipitation fields.

The clustering procedure followed the hierarchical Ward's method, which minimizes total within-cluster variance by reducing the sum of squared differences based on Euclidean distance as the dissimilarity metric. This approach, as described by [17] and adopted in several climate regionalization studies [28–31], is effective for identifying groups with high internal homogeneity and distinct inter-cluster variability. The within-cluster sum of squares is expressed as:

$$W = \sum_{k=1}^{K} \sum_{i \in C_k} (x_i - \mu_k)^2 \quad (1)$$

where K is the number of clusters, C_k is the set of points in cluster k, μ_k is the mean of the points in cluster k.

To visualize the clustering results, a dendrogram was produced, representing the hierarchical structure of the formed clusters. The dendrogram helps identify groupings and determine the optimal number of clusters [32].

Additionally, the quality of the clustering was assessed using the cophenetic correlation coefficient. This coefficient measures the correlation between the actual pairwise distances and the cophenetic distances derived from the dendrogram, and is calculated as follows:

$$r_c = \frac{\sum_{i<j} \left(d_{ij} - \overline{d}\right)\left(t_{ij} - \overline{t}\right)}{\sqrt{\sum_{i<j} \left(d_{ij} - \overline{d}\right)^2 \sum_{i<j} \left(t_{ij} - \overline{t}\right)^2}} \quad (2)$$

where

d_{ij} = Euclidean distance between points i and j,
t_{ij} = Cophenetic distance between points i and j,
$\overline{d}$ e $\overline{t}$ = Mean Euclidean and cophenetic distances, respect.

A cophenetic coefficient approaching 1 indicates good clustering quality [32]. However, Romesburg [33] notes there are no exact guidelines for defining an "adequate" cophenetic coefficient, as its acceptability depends on context and data complexity. In many studies, values above 0.8 are desirable, although slightly lower values may still be acceptable, especially with highly variable climatic or spatial data. Hence, this coefficient serves as a quality indicator but should be interpreted cautiously.

The clusters derived allowed detailed analysis of IMERG V06 and V07 satellite-derived precipitation estimates, enabling a better understanding of spatial and temporal precipitation variability within the PRB. These clusters will be fundamental for future bias-correction analyses and modeling the probability of extreme precipitation events in the region.

2.3.3. Evaluation Metrics

To assess the performance of precipitation estimates, multiple statistical and detection-based metrics were applied, encompassing event identification, error magnitude, and correlation measures. Detection metrics evaluate the ability of the product to correctly identify precipitation events. These include the Probability of Detection (POD) and the False Alarm Ratio (FAR), which indicate, respectively, the fraction of observed events correctly detected and the proportion of false detections. Both metrics follow the definitions proposed by Wilks [34] and are summarized in Table 1.

Table 1. Evaluation metrics.

Metric	Equation	Perfect Value	Unit	
Probability of detection (POD)	$POD = H \,/\, (H + M)$	1	—	(3)
False alarm ratio (FAR)	$FAR = F \,/\, (H + F)$	0	—	(4)
Correlation coefficient (CC)	$CC = \frac{\sum_{i=1}^{n}\left(P_i^s - \overline{P}^s\right)\left(P_i^r - \overline{P}^r\right)}{\sqrt{\sum_{i=1}^{n}\left(P_i^s - \overline{P}^s\right)^2}\sqrt{\sum_{i=1}^{n}\left(P_i^r - \overline{P}^r\right)^2}}$	1	—	(5)
Root-mean-square error (RMSE)	$RMSE = \sqrt{MSE} = \sqrt{\frac{1}{n}\sum\left(P_i^s - P_i^r\right)^2}$	0	mm	(6)
Relative bias	$RBias = \left(\frac{\sum_{i=1}^{n}(P_i^s - P_i^r)}{\sum_{i=1}^{n} P_i^r}\right) \times 100$	0	%	(7)
Random Error	$RE = \sqrt{MSE - SE} = \sqrt{\frac{1}{n}\sum\left(P_i^s - P_i^r\right)^2 - \left(\overline{P}^s - \overline{P}^r\right)^2}$	0	%	(8)
Kling-Gupta Efficiency (KGE)	$KGE = 1 - \sqrt{(CC-1)^2 + (\beta-1)^2 + (\gamma-1)^2}$	1	—	(9)

Notes: Where P_i^s is the estimated value, P_i^r is the reference value, and $\underline{P}^s$ and $\underline{P}^r$: are the mean estimated and mean reference values, respectively. H (Hits): Correctly predicted observed events. M (Misses): Observed events that were not predicted and F (False Alarms): Predicted events that did not occur.

Statistical metrics were utilized to assess precipitation estimation accuracy. The Mean Relative Bias (RBias %) measures the average relative difference between estimates and observations, indicating systematic underestimation or overestimation. The Correlation Coefficient (CC) quantifies the strength of the linear relationship between estimates and observations. The Root-Mean-Square Error (RMSE) evaluates average error magnitude, emphasizing larger errors. The Normalized Mean Absolute Bias (NMAB %) represents relative error without considering direction, reflecting general accuracy. Random Error (RE %) quantifies absolute error variability. Finally, the Kling-Gupta Efficiency (KGE) integrates correlation, bias, and variability, providing a comprehensive evaluation of model performance.

The mathematical formulations of all metrics used in this study are presented in Table 1 [34].

In addition to performance metrics, non-parametric statistical tests were employed to assess the significance of differences in accuracy indicators. The Kruskal–Wallis test was used to evaluate inter-cluster variability in the Kling–Gupta Efficiency (KGE), Root Mean Square Error (RMSE), and Mean Absolute Error (MAE). Pairwise comparisons between IMERG V06 and V07 were subsequently performed using the Wilcoxon rank-sum test. These tests were selected because the performance metrics violated the assumptions of normality (Shapiro–Wilk, $p < 0.001$) and homogeneity of variance (Levene's test, $p < 0.001$), making non-parametric approaches more appropriate. Statistical significance was assessed at the 5% level.

3. Results

3.1. Assessment of Reference Data

Figure 3a presents a comparative analysis between the daily precipitation estimates from the BR-DWGD product and the observational data from 58 rain gauges distributed across the PRB. A strong correlation (r = 0.81) is observed for daily data, despite the dispersion seen in high precipitation events, indicating the need for adjustments under extreme conditions. This finding is consistent with Xavier et al. [21], who highlighted that microclimatic complexity and high spatial variability impose limitations on accurately capturing intense precipitation events using BR-DWGD at daily scales. Monthly totals were obtained by summing daily precipitation values, and this comparison was included

to illustrate the improved consistency of the product at coarser temporal resolution. In the monthly analysis (Figure 3b), an even stronger correlation is observed (r = 0.95), indicating that the BR-DWGD product performs better in estimating monthly precipitation averages. This result reinforces its application for regional-scale and long-term analyses, in accordance with the findings of Bender and Sentelhas [26].

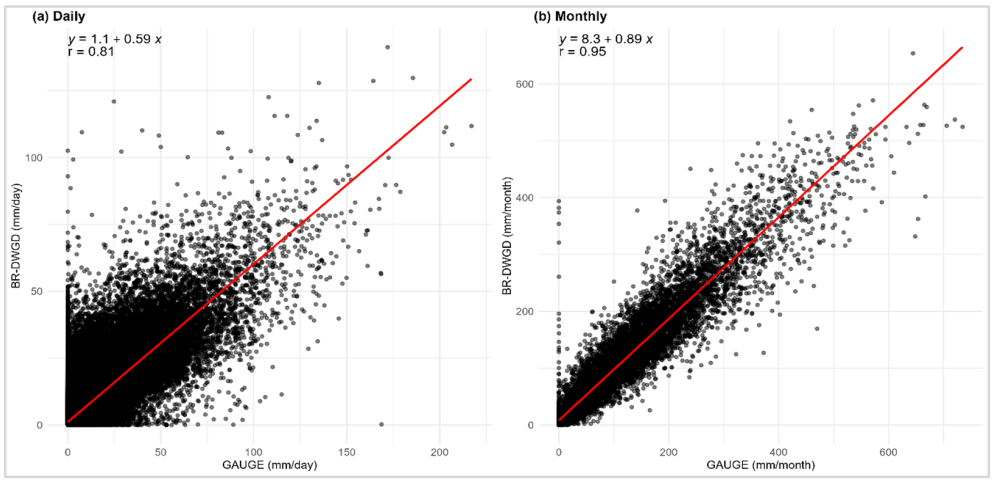

Figure 3. Scatterplots between estimated (BR-DWGD) and observed (Gauge) daily (**a**) and monthly precipitation data (**b**). The red line indicates the 1:1 reference line (perfect agreement between observed and estimated values).

Figure 4a presents the results of the comparison between precipitation data observed by rain gauges (in green) and the interpolated data from BR-DWGD (in red). It is observed that the product follows the seasonal variability of the observed precipitation data well, although it exhibits a slight underestimation during the rainy season, especially from January to April.

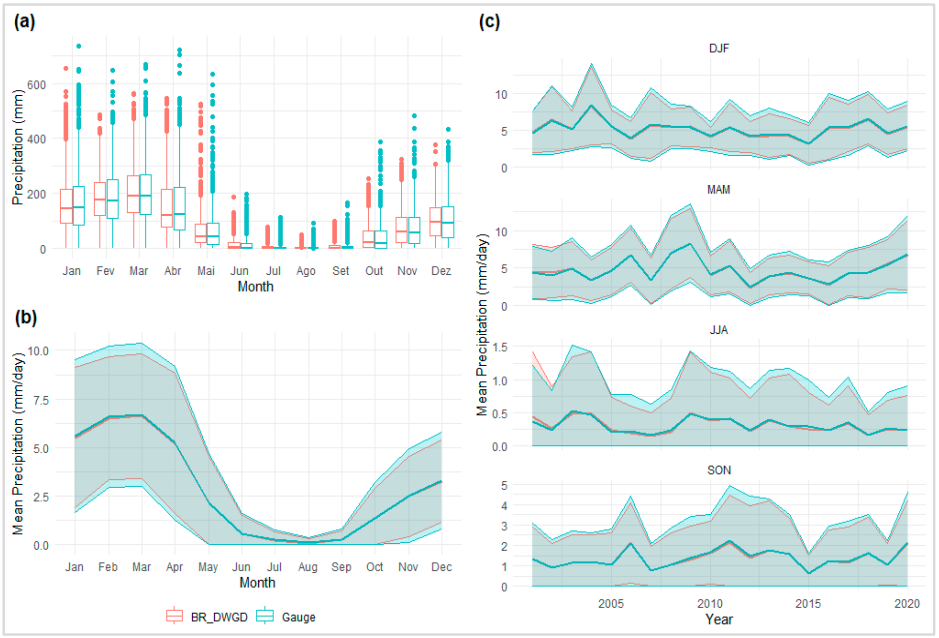

Figure 4. (**a**) boxplot of total monthly accumulated precipitation, (**b**) mean monthly precipitation with standard deviation, and (**c**) mean seasonal precipitation (DJF, MAM, JJA, SON) for the Parnaíba basin, comparing observed (Gauge) and gridded (BR-DWGD) data. The red color represents BR-DWGD estimates, while the green color represents gauge observations.

Figure 4b,c present the mean monthly and seasonal precipitation, respectively, highlighting intra-annual and inter-annual precipitation variability. A broader variability range is noted during rainy months, indicating higher uncertainty associated with precipitation estimates for this period. Gauge data capture this variability more effectively, whereas BR-DWGD tends to smooth out the estimates, particularly during months of intense rainfall. Nevertheless, BR-DWGD shows greater accuracy during dry seasons (JJA and SON), reinforcing its utility for seasonal analyses.

The complexity of precipitation patterns in Northeast Brazil (NEB) is strongly influenced by large-scale phenomena such as El Niño and La Niña, which substantially modulate interannual variability and the seasonal distribution of rainfall [35]. These phenomena account for part of the discrepancies observed in the plots, particularly during the rainy season. Although the BR-DWGD product tends to smooth extreme precipitation events, it remains a valuable dataset for identifying large-scale climate patterns and supporting water resource management, especially in semi-arid regions [20].

Table 2 presents a comparison between BR-DWGD daily precipitation estimates and observational gauge data in the Parnaíba Basin. The results show good annual correspondence, with close mean values (2.83 $\pm$ 6.85 mm/day for observations and 2.86 $\pm$ 9.40 mm/day for BR-DWGD) and a positive bias of only 0.03 mm/day (1.17%). The greater variability observed in the gridded data (sd = 9.40 vs. 6.85 mm/day) may reflect both the sensitivity of the interpolation method and the climatic complexity of the region, which encompasses different precipitation regimes due to its territorial extent and marked seasonality.

Table 2. Comparison between BR-DWGD daily precipitation estimates and observed precipitation data for the period 2001–2020 in the PRB, aggregated across all months and individual seasons. Values represent mean daily precipitation (mm/day) averaged across the 58 rain gauge locations and aggregated by climatological season. Numbers in brackets refer to standard deviation (sd).

	Observed Precipitation (Mean, sd) (mm/Day)	**Estimated (BR-DWGD) (Mean, sd) (mm/Day)**	**Bias (mm/Day)**	**Relative Bias (%)**	**RMSE (mm/Day)**	**Correlation**
Annual	2.83 (6.85)	2.86 (9.40)	0.03	1.17	5.53	0.81
DJF	5.01 (8.82)	5.09 (12.36)	0.07	1.44	7.46	0.80
MAM	4.66 (8.04)	4.70 (11.31)	0.03	0.73	6.84	0.79
JJA	0.30 (1.41)	0.30 (1.98)	0.00	1.34	1.29	0.75
SON	1.35 (4.36)	1.36 (6.27)	0.02	1.69	3.79	0.79

During rainy seasons (DJF and MAM), bias and RMSE values increase significantly (7.46 mm/day in DJF and 6.84 mm/day in MAM), reflecting an overestimation tendency during high-precipitation events caused by smoothing of maximum and minimum values. In contrast, during dry seasons (JJA and SON), bias and RMSE values decrease, reflecting higher accuracy of BR-DWGD under conditions of lower precipitation. The lowest RMSE is recorded in winter (JJA), at 1.29 mm/day, along with variability similar to observational data (sd of 1.98 mm/day vs. 1.41 mm/day in JJA), corresponding to a difference of only 0.57 mm/day (~ 40%). This close agreement facilitates interpolation and enhances accuracy during periods of reduced variability.

The correlations obtained, consistently above 0.7, indicate a robust relationship between BR-DWGD estimates and observational data. Additionally, the relative bias recorded remained below 2%, demonstrating satisfactory accuracy in representing precipitation, particularly under moderate variability conditions.

The results indicate that BR-DWGD is effective for representing seasonal and annual averages, making it useful for long-term climate analyses. Alternatively, the product tends

to underestimate precipitation during the rainy season, particularly under high-intensity events. To address these spatial discrepancies, the subsequent analysis considers the basin divided into homogeneous clusters based on precipitation behavior, improving the ability to capture local variability and assess satellite performance across distinct climatic zones.

3.2. Evaluation of IMERG V07 Versus V06

Figure 5 (a) MAE, (b) RMSE, (c) Correlation, (d) KGE—together with Table 3, present the comparative analysis between IMERG V06 and V07 versions against BR-DWGD data in the PRB. Overall, IMERG V07 exhibited a reduced MAE and RMSE in the central and southern areas of the basin compared to V06. During the MAM season, version V07 achieved an SE of 5.356 compared to 7.396 for V06, as indicated in Table 3. However, during the JJA season, biases remained high for both versions, mainly in the northern sector of the basin, which showed greater rainfall variability.

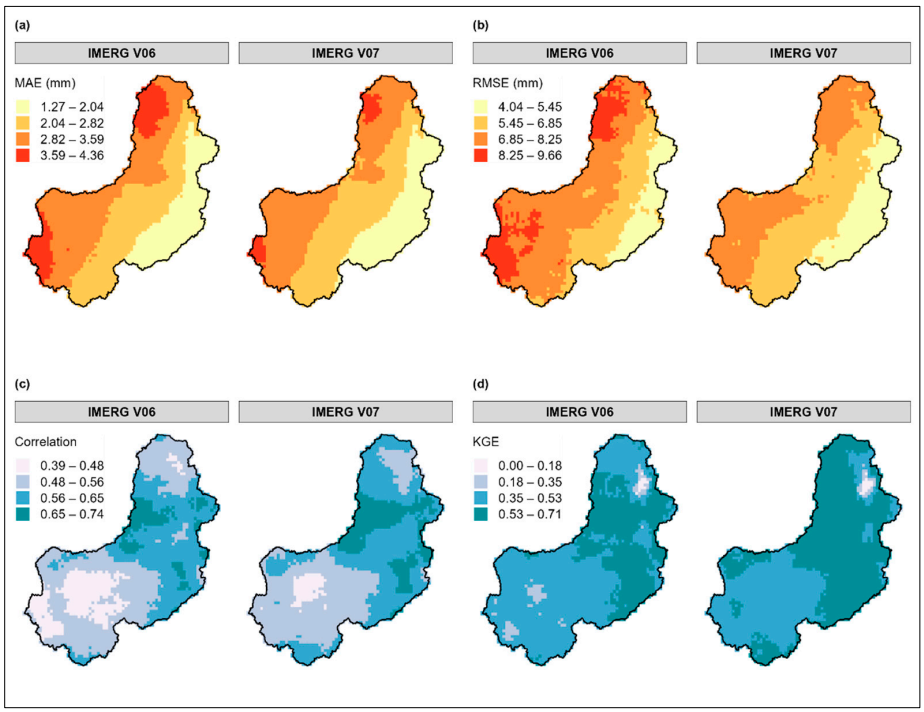

Figure 5. Spatial distribution of evaluation metrics between IMERG V06 and V07 compared with BR-DWGD daily precipitation in the Parnaíba basin (2001–2020). (**a**) Mean absolute error (MAE); (**b**) root mean square error (RMSE); (**c**) correlation coefficient; (**d**) Kling-Gupta efficiency (KGE).

Table 3. Comparison of efficiency metrics between IMERG V06 and V07 relative to BR-DWGD reference precipitation data for the period 2001–2020 in the PRB, aggregated by months and all pixels. metrics computed from daily data and aggregated by month.

Metric	IMERG (Version)	DJF	MAM	JJA	SON	Annual
RBias (%)	V07	7.76	5.36	14.3	11.4	7.4
	V06	10.6	7.4	28.9	11.9	9.85
RE (%)	V07	98.2	95.9	140.0	118.0	100.64
	V06	104.0	100.0	152.0	122.0	105.58
RMSE	V07	8.83	7.81	1.56	4.96	6.43
	V06	9.83	8.7	1.73	5.41	7.14

Table 3. *Cont.*

Metric	IMERG (Version)	DJF	MAM	JJA	SON	Annual
KGE	V07	0.532	0.557	0.476	0.500	0.572
	V06	0.475	0.492	0.406	0.456	0.516
CORR	V07	0.545	0.574	0.498	0.515	0.586
	V06	0.515	0.538	0.483	0.485	0.553
BETA	V07	1.077	1.053	1.143	1.113	1.073
	V06	1.105	1.073	1.288	1.118	1.098
GAMMA	V07	1.079	1.108	1.045	1.044	1.077
	V06	1.170	1.196	1.046	1.130	1.158
POD (%)	V07	0.697	0.665	0.385	0.583	0.732
	V06	0.681	0.662	0.392	0.561	0.753
FAR (%)	V07	0.276	0.252	0.633	0.428	0.277
	V06	0.267	0.253	0.645	0.425	0.293

The analysis of correlation (Figure 5c) and Kling–Gupta Efficiency (KGE) (Figure 5d) metrics reinforces the superior performance of IMERG V07, particularly in the central and southern regions of the basin where climatic variability is relatively more moderate. As shown in Figure 5d and Table 3, V07 achieved an annual KGE value of 0.572, higher than the 0.516 recorded for V06, indicating a greater ability to capture the seasonal variability of precipitation. The correlation coefficients of V07 ranged from 0.545 during the DJF season to 0.586 annually, consistently surpassing those of V06, which varied between 0.515 and 0.553. These results indicate that IMERG V07 provides a more consistent representation of precipitation across most of the basin.

POD (Figure 6a) and FAR (Figure 6b) metrics presented in Figure 6 show that although V07 exhibits a slightly lower average POD (0.732 versus 0.753 for V06), demonstrating higher efficacy in precipitation detection due to its lower FAR (0.277 versus 0.293). This improved performance reflects the advancements in V07, notably in reducing false alarms and capturing precipitation variability in regions with high rainfall accumulations, such as the basin's central and northern areas, where moisture from the Amazon intensifies convective systems and deep cloud formation.

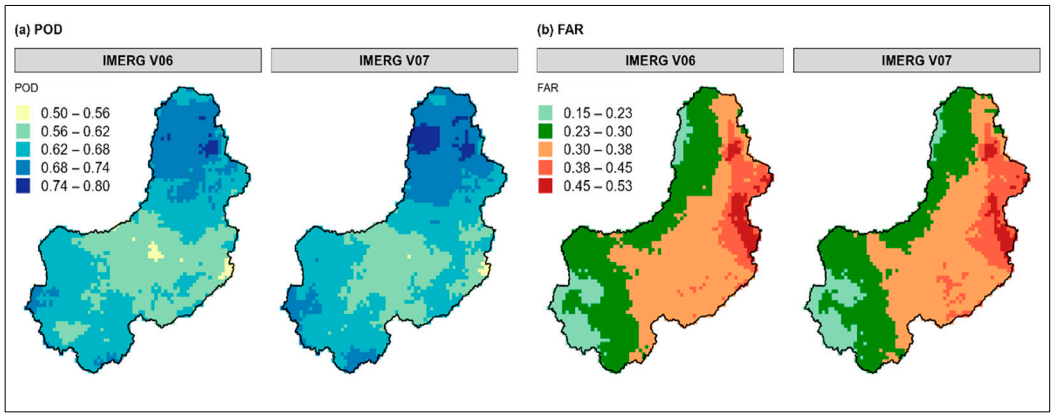

Figure 6. Spatial maps of detection metrics (**a**) POD and (**b**) FAR between IMERG V06 and V07 compared with BR-DWGD precipitation in the Parnaíba Basin (2001–2020).

Figure 7 shows the spatial maps of Relative Bias (Rbias %) and Random Error (RE %) comparing IMERG versions V06 and V07 in the Parnaíba Basin. A pronounced reduction in Rbias is evident, especially in the central and southern regions, where values decreased from 60–80% (V06) to 20–40% (V07). During the rainy period of March to May (MAM), V07 shows a significant reduction in Rbias compared to V06 (Table 3). Despite these advances, high Rbias values (>70%) and Random Error exceeding 150% persist in the basin's northeastern highlands, indicating continuing limitations even in V07.

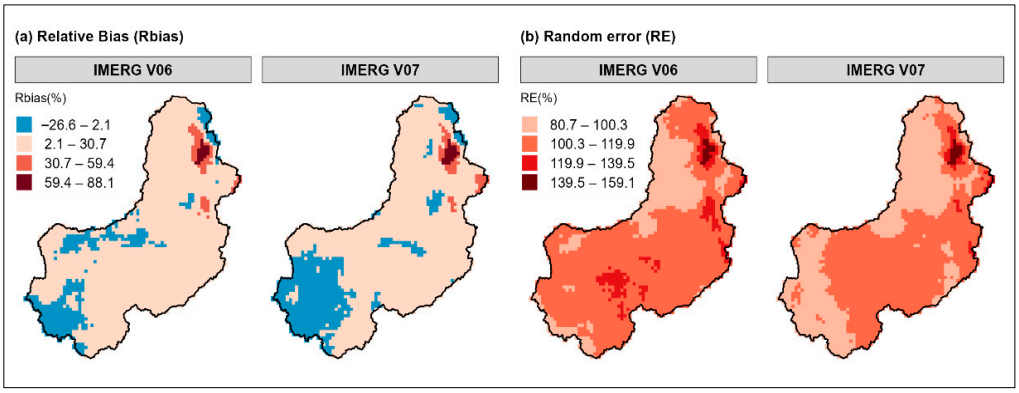

Figure 7. Spatial maps of systematic and random error metrics from IMERG V06 and V07 compared with BR-DWGD daily precipitation in the Parnaíba basin (2001–2020). (**a**) Relative bias (Rbias %); (**b**) random error (RE %).

Results presented in Figures 5 and 6, and Table 3 indicate significant advancements by IMERG V07 in representing precipitation in the Parnaíba Basin, particularly through bias reduction, increased precision (RMSE), and improved detection of precipitation events (POD and FAR). These improvements can be attributed to enhanced calibration algorithms in V07, which better adjust estimates in regions of high climatic variability, such as northeastern Brazil's semi-arid region.

The observed improvements in Version 7, alongside persisting limitations, underscore the importance of continuous advancements to address the climatic and topographic complexity of the Parnaíba Basin and surrounding areas. The interplay of climate systems such as cold fronts in the South and the ITCZ in the North creates a mosaic of rainfall variability across diverse terrains, necessitating high-precision models. Recent enhancements in IMERG V07 render it an essential tool for hydrological and climate studies, providing a more reliable basis for precipitation analysis in tropical regions. Nevertheless, areas characterized by high humidity and frequent convection, such as northern MATOPIBA and the Parnaíba Basin, still require further data-processing advancements, particularly to capture extreme precipitation in continuously changing climatic and topographic environments.

3.3. Comparative Analysis by Cluster

The determination of the optimal number of clusters was supported by the combined analysis of quantitative and visual criteria. As shown in Figure 8, Ward's hierarchical dendrogram (Figure 8a) delineated four main groups, with the cut-off level set at a linkage distance of approximately 20,000, as indicated by the red dashed line. This configuration was consistent with the elbow method (Figure 8b), which displayed an inflection point at k = 4, and produced the highest cophenetic correlation coefficient (0.68 for BR-DWGD), confirming the best structural consistency. The spatial distribution of the resulting regions (Figure 8c) further demonstrated coherent and climatically meaningful boundaries across the basin. Together, these complementary criteria indicate that four clusters adequately represent the rainfall regimes of the Parnaíba River Basin (PRB).

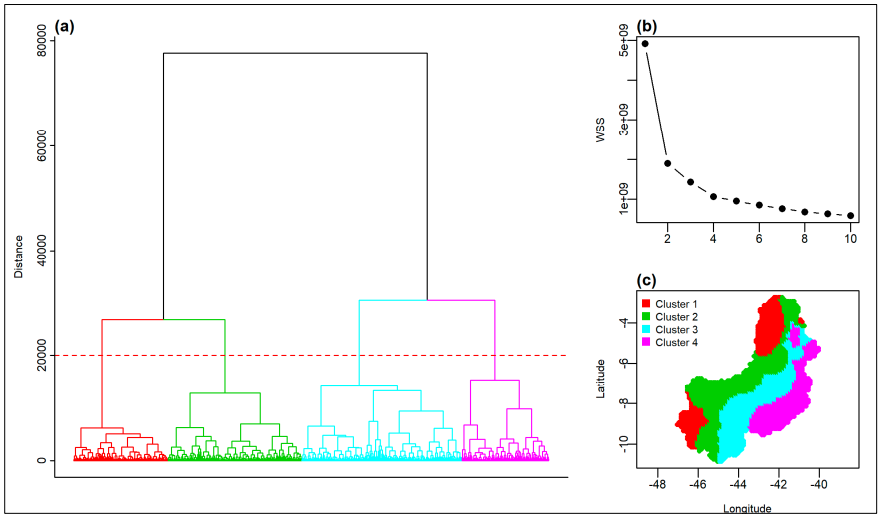

Figure 8. Homogeneous regions for the Parnaíba river basin (2001–2020) based on BR-DWGD data: (**a**) dendrogram using Ward's method, with the red line indicating the four-cluster cut-off; (**b**) elbow method showing the inflection at $k = 4$; and (**c**) spatial distribution of the resulting homogeneous precipitation regions.

The final configuration with four homogeneous clusters was adopted for subsequent analyses. The cophenetic correlation coefficients obtained were 0.68 for BR-DWGD, 0.62 for IMERG V06, and 0.64 for IMERG V07, indicating moderate yet acceptable clustering stability within a basin characterized by high climatic heterogeneity [33]. These values are consistent with those reported in previous precipitation regionalization studies conducted in complex climatic domains, confirming the robustness of the adopted classification.

Figure 9 illustrates the spatial delineation of these four homogeneous clusters and their correspondence with the BR-DWGD and IMERG datasets. The observed improvement in IMERG V07 relative to V06 suggests that algorithmic refinements enhanced the spatial representation of precipitation patterns, particularly in transitional and semi-arid regions.

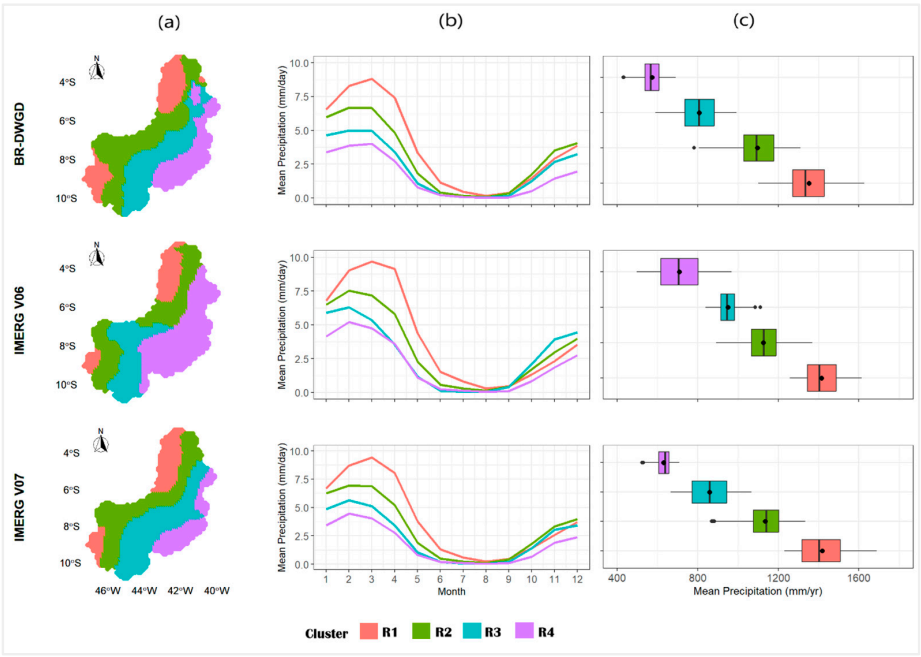

Figure 9. Cluster Analysis (Ward's Method) and Precipitation in the Parnaíba Basin (2001–2020): (**a**) Definition of Homogeneous Regions, (**b**) Seasonal Patterns of Mean Monthly Precipitation by Cluster, (**c**) Distribution of Mean Annual Precipitation.

Examining the cluster distribution maps, Cluster R1—characterized by the highest rainfall accumulations—is well-represented by IMERG V07, whereas Cluster R4, covering the semi-arid region, also shows improved estimation accuracy in areas with lower precipitation. Cluster R3, representing a transitional zone, also stands out for better capturing seasonal and spatial variations.

In the southern regions of Clusters R2 and R3, encompassing the MATOPIBA region, climatic features are complex, influenced by the South Atlantic Convergence Zone (SACZ) and moisture transport from the Amazon. IMERG V07 demonstrated a significant enhancement in precipitation estimation accuracy within these clusters due to algorithmic corrections, including rectification of geolocation errors and adjustments to correct systematic biases, as described by [5]. These enhancements resulted in improved detection capabilities and a more realistic representation of observed rainfall patterns, essential for regions with high climatic variability [5,8].

The seasonal patterns of mean monthly precipitation by cluster (Figure 9b) also show greater similarity between IMERG V07 and BR-DWGD, with curves closely matching the seasonal trends captured by the reference dataset. During the rainy season (DJF), V07 values for Clusters 1 and 4 are better aligned with BR-DWGD compared to V06, suggesting improved detection of rainfall intensity and distribution. Conversely, V06 tends to overestimate precipitation in certain regions and seasons, resulting in patterns less consistent with BR-DWGD.

Table 4 reinforces the comparative analysis findings, demonstrating that IMERG V07 exhibits daily mean precipitation values closer to the BR-DWGD reference data and reduced variability in errors. For instance, in Cluster R1 during the rainy period (DJF), the mean value for V07 is 6.3 mm/day, closely matching the 6.16 mm/day observed in BR-DWGD, while V06 shows 6.43 mm/day, indicating slight overestimation. During the dry season (JJA), V07 also better approximates the reference values. Specifically, in Cluster R1, V07 corrects the V06 overestimation (0.87 mm/day), presenting 0.69 mm/day, closer to BR-DWGD's 0.58 mm/day. Similarly, in Cluster R3, where V06 underestimated (0.08 mm/day), V07 adjusts to 0.10 mm/day, practically identical to the BR-DWGD value of 0.11 mm/day.

Table 4. Comparison of IMERG V06 and V07 with BR-DWGD data in the Parnaíba basin: mean daily precipitation (mm/day) and standard deviation by homogeneous regions and seasonality.

Cluster Region		DJF	MAM	JJA	SON
R1	BR-DWGD	6.16 (9.23)	6.51 (9.37)	0.58 (2.39)	1.58 (4.86)
	IMERG V06	6.43 (11.54)	7.73 (13.18)	0.87 (3.68)	1.35 (5.35)
	IMERG V07	6.3 (10.54)	7.07 (11.25)	0.69 (3.09)	1.48 (5.11)
R2	BR-DWGD	5.54 (8.93)	4.43 (7.91)	0.21 (1.39)	1.87 (5.60)
	IMERG V06	5.99 (11.73)	5.08 (10.47)	0.34 (2.03)	1.69 (6.23)
	IMERG V07	5.69 (10.41)	4.66 (9.24)	0.27 (1.73)	1.85 (6.08)
R3	BR-DWGD	3.14 (6.69)	4.27 (8.02)	0.11 (0.97)	1.36 (4.75)
	IMERG V06	3.35 (8.66)	5.55 (11.38)	0.08 (0.89)	2.12 (7.28)
	IMERG V07	3.19 (7.70)	4.61 (9.23)	0.10 (0.95)	1.54 (5.43)
R4	BR-DWGD	3.05 (7.26)	2.50 (6.06)	0.10 (0.90)	0.66 (3.30)
	IMERG V06	4.02 (9.57)	3.16 (8.23)	0.14 (1.18)	0.93 (4.37)
	IMERG V07	3.38 (8.14)	2.55 (6.93)	0.11 (1.02)	0.87 (4.18)

Algorithmic corrections implemented in V07 result in enhanced estimation accuracy during both high- and low-precipitation periods (Table 4), contributing to a more consistent precipitation representation essential for climatic and hydrological studies. For example, during the rainy season (DJF) in Cluster R2, V07 shows an average of 5.69 mm/day (standard deviation 10.41), closer to BR-DWGD's 5.54 mm/day (8.93), while V06 averages 5.99 mm/day (11.73), indicating higher variability. In the dry season (JJA), improvement is even more evident, with V07 reducing the average to 0.27 mm/day (1.73), aligning closely with BR-DWGD's 0.21 mm/day (1.39), and displaying lower standard deviation compared to V06, which has 0.34 mm/day (2.03). Nonetheless, overestimation still occurs in some instances, such as in Cluster R2 during SON, where V07 records 1.85 mm/day (6.08), slightly above BR-DWGD's 1.87 mm/day (5.60), but still showing reduced variability compared to V06, which reports 2.03 mm/day (6.23).

The improved accuracy of V07 in both dry and rainy seasons, evidenced by its closer alignment to BR-DWGD data (Table 4), is consistent with findings by Rozante and Rozante [11], who demonstrated that V07 reduces both overestimations in convective systems (as in the summer for region R2) and underestimations in semi-arid regions (as in the winter for region R3). These advancements result from incorporating enhanced calibration datasets and refining the Kalman filtering algorithm in V07 [5].

3.4. Inter-Cluster Comparison

Figure 10 presents the performance of IMERG versions V06 and V07 across the four homogeneous clusters, evaluated using the MAE, RMSE, Correlation, and Kling–Gupta Efficiency (KGE) metrics. Among these, KGE was selected as the main comparative indicator, as it integrates correlation, bias, and variability components into a single index, providing a more comprehensive measure of performance consistency.

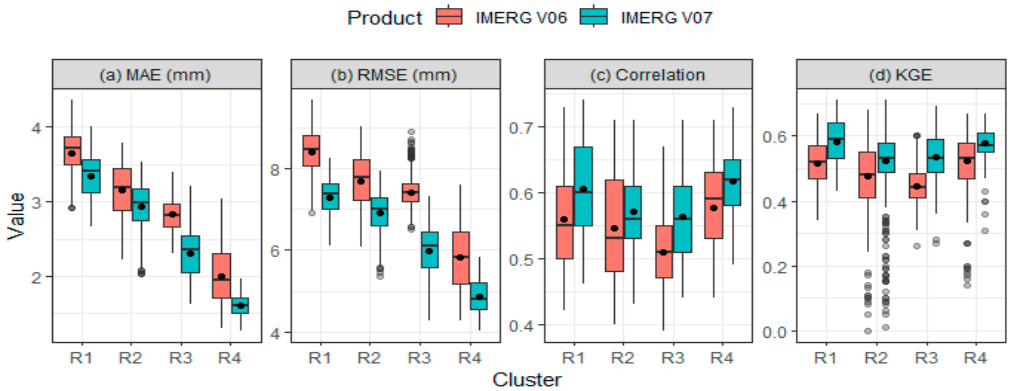

Figure 10. Boxplots of performance metrics ((**a**) MAE, (**b**) RMSE, (**c**) Correlation, and (**d**) KGE) for IMERG V06 and V07 across four homogeneous clusters in the Parnaíba River Basin.

To determine whether the differences observed among clusters and between IMERG versions were statistically significant, nonparametric tests were applied. The Kruskal–Wallis test revealed significant inter-cluster variability in KGE for both versions (χ^2 = 162.3 for V06 and 73.2 for V07; $p < 0.001$), confirming that precipitation estimation performance varies with the basin's climatic heterogeneity.

Pairwise comparisons using the Wilcoxon rank-sum test (Table 5) confirmed that IMERG V07 achieved significantly higher KGE values than V06 in all clusters ($p < 0.001$), with mean KGE improvements ranging from 0.05 to 0.07. These consistent and statistically significant differences demonstrate that the algorithmic refinements implemented in IMERG V07 resulted in spatially coherent performance gains across the basin.

Table 5. Wilcoxon rank-sum test results for KGE between IMERG V06 and V07 by cluster.

Cluster	Mean KGE (sd) (IMERG V06)	Mean KGE (sd) (IMERG V07)	W Statistic	*p*-Value
R1	0.485 (0.079)	0.558 (0.065)	63,952.5	<0.001
R2	0.485 (0.085)	0.544 (0.076)	264,005.0	<0.001
R3	0.484 (0.078)	0.537 (0.066)	178,577.0	<0.001
R4	0.522 (0.098)	0.550 (0.106)	108,399.5	<0.001

Table 5 presents the results of the Wilcoxon rank-sum test comparing Kling–Gupta Efficiency (KGE) values between IMERG V06 and V07 for the four homogeneous clusters identified in the Parnaíba River Basin. Mean and standard deviation (SD) are reported for each version, providing a quantitative basis for assessing the magnitude of improvement in the latest release.

The combined evidence from boxplots (Figure 10) and hypothesis tests demonstrates that IMERG V07 provides lower random errors (MAE, RMSE) and higher KGE and correlation values across all clusters. These results indicate that the improvements achieved in V07 are statistically robust and spatially consistent across the basin's diverse climatic regimes.

4. Discussion

This study adopted a stepwise methodological framework, beginning with the validation of the BR-DWGD product against 58 rain gauges to establish a reliable reference for evaluating IMERG products on a daily scale over the Parnaíba River Basin (PRB). Although BR-DWGD is a high-quality interpolated dataset, it presents inherent limitations related to interpolation techniques, particularly in representing extreme daily rainfall events, as evidenced by the dispersion of higher values (Figure 3a). These findings align with Xavier et al. [21] and Bender & Sentelhas [26], who highlighted the difficulty of interpolated products in capturing intense convective rainfall at micro scales, especially in regions with pronounced topographic heterogeneity. Similar behaviors have also been reported in complex tropical and mountainous environments ([36,37]), where smoothing of extreme values during high-precipitation periods is a recurrent feature of interpolation-based datasets. Nevertheless, previous national assessments [38,39] have recognized BR-DWGD as the most reliable spatially distributed reference dataset derived from in situ measurements, making its use as a baseline for IMERG evaluation both valid and methodologically sound.

The performance improvements identified for IMERG V07 in the PRB—particularly the reduction in systematic bias, decrease in false alarms, and higher Kling–Gupta Efficiency (KGE)—are consistent with global trends observed in recent evaluations. Rozante & Rozante [11] reported similar reductions in false alarms and improved correlation for V07 across Brazil, while Guo et al. [6] and Tang et al. [4] documented comparable increases in KGE and decreases in RMSE over complex terrain in China and Southeast Asia. The convergence between these studies and the present results reinforces that the improvements observed in the PRB are not localized but rather part of a broader global enhancement achieved through the V07 reprocessing.

Previous analyses of the IMERG V6 product for the same basin by Batista et al. [40] demonstrated that, although IMERG Final showed satisfactory performance for several ETCCDI indices such as PRCPTOT, RX5day, and CDD, systematic biases and underestimations of intense rainfall events persisted, particularly in regions with complex topography and warm-top convective systems. Similar results were also reported by dos Santos et al. [41], who evaluated IMERG V6 over Brazil's semiarid region and found that the prod-

uct tended to underestimate extreme precipitation indices, especially in areas influenced by convective rainfall and low rain gauge density. These findings highlighted the need for further evaluation of the reprocessed IMERG V07 algorithm to determine whether the observed biases could be reduced and detection metrics improved at the basin scale.

When comparing IMERG V07 and V06 across clusters and seasons, the results clearly indicate systematic improvements in detection performance. These advancements are particularly evident in the central and southern regions of the basin, where reductions in systematic bias and false alarms (Figure 5, Table 4) reflect the enhanced capability of V07 to reproduce daily rainfall variability. The statistically significant differences confirmed by non-parametric tests ($p < 0.001$; Table 5) demonstrate that these improvements are consistent and spatially coherent, reinforcing the robustness of the updated algorithm in diverse climatic settings. This season-dependent performance aligns with findings by Xu et al. [42], who observed similar challenges in representing extreme rainfall variability during wet seasons in the Pearl River Basin, emphasizing the sensitivity of satellite products to high temporal and spatial variability in convective environments.

The cluster-based regionalization provided additional insights into the spatial consistency of these improvements. During the rainy season (DJF), V07 more accurately represented rainfall intensity and distribution in Cluster R1, the basin's wettest region, while in the dry season (JJA), it corrected the V06 overestimation (0.69 mm/day versus 0.58 mm/day in BR-DWGD). Similar improvements were observed in transitional regions (R2 and R3), influenced by the South Atlantic Convergence Zone (SACZ) and moisture advection from the Amazon, confirming that the algorithmic corrections in V07 yielded spatially coherent enhancements across distinct climatic regimes. This approach aligns with previous applications of cluster-based regionalization in the Brazilian semi-arid region [43] and Piauí region [44], which demonstrated improved representation of spatial rainfall variability through the identification of homogeneous precipitation zones. The statistical tests (Kruskal–Wallis and Wilcoxon rank-sum) further demonstrated that these improvements are significant ($p < 0.001$) and spatially consistent across all clusters (Table 5), highlighting the robustness of the results.

Despite these advances, persistent limitations remain in the highland areas of northeastern PRB, where Relative Bias (Rbias > 70%) and Random Error (RE > 150%) remain elevated. These residual errors reflect the challenges of satellite retrieval in orographically complex environments. The combination of error mechanisms includes (i) microwave signal attenuation and orographic shadowing that cause partial underestimation; (ii) misclassification by infrared retrievals between cold cloud tops and cold land surfaces; and (iii) limitations of global calibration schemes that fail to capture localized rainfall gradients. Similar difficulties have been reported for semi-arid regions of Northeast Brazil [11], climatic transition zones in China [6 mountainous basins in southwestern China [45], and steep terrains in southwestern Europe [46–48]. Such consistency reinforces that terrain-induced retrieval errors are a global limitation not yet fully overcome by current satellite algorithms.

The results validate IMERG V07 as a substantially improved tool for hydrological and climate applications requiring daily rainfall data in northeastern Brazil. The consistency between cluster-level improvements and statistical significance tests confirms that these advances are robust rather than regionally isolated. By integrating hierarchical clustering with a multi-scale validation framework, this study provides a spatially explicit understanding of IMERG performance across different climatic zones of the Parnaíba Basin. Furthermore, it represents the first basin-scale evaluation of IMERG V07 using a cluster-based regionalization approach in northeastern Brazil, contributing to global validation efforts and

offering methodological insights for future satellite rainfall assessments in semi-arid and topographically complex environments.

5. Conclusions

The comparative analysis between IMERG Final versions V06 and V07 demonstrates significant advancements in V07 regarding precipitation estimation accuracy and systematic error reduction. Version V07 closely approximates the BR-DWGD reference data, especially in areas of rugged topography and high seasonal variability, such as the basin's central and southern regions. In contrast, V06 tends to overestimate precipitation in some areas, indicating systematic biases partially corrected in V07, resulting in more consistent estimates with reduced biases.

Version V07 also reduces the variability of random errors, as evidenced by lower standard deviations across multiple seasons and clusters. This improvement in estimation consistency is particularly evident during the rainy season (DJF), when regional systems such as the Intertropical Convergence Zone (ITCZ) and moist air masses from the Amazon enhance precipitation within the basin. The superior performance of V07 in capturing regional atmospheric features and seasonal patterns underscores its suitability for seasonal monitoring in areas characterized by high climatic complexity.

Nevertheless, challenges persist, particularly in dry periods (JJA) and regions with low rainfall, where both V06 and V07 exhibit underestimations. This indicates the need for further adjustments to accurately capture low precipitation volumes under these conditions. Future studies could explore the application of bias corrections specifically tailored to the Parnaíba Basin, leveraging the homogeneous clusters already established to regionally address systematic and random errors. This cluster-based correction approach would allow for the development of targeted bias adjustments, considering the distinct climatic and topographic characteristics of each region. Such regionalized corrections would yield more robust and reliable precipitation estimates, significantly enhancing IMERG's utility for hydrological analyses.

Although the methodological framework ensured robust and spatially consistent results, some limitations should be acknowledged. The accuracy of the BR-DWGD reference data depends on the spatial distribution of rain gauges and on the smoothing effect inherent to interpolation, especially during high-precipitation periods. In addition, the IMERG evaluation was performed at a daily scale, which may not capture short-lived convective events occurring at sub-daily intervals. Finally, residual uncertainties remain in mountainous regions due to orographic effects and the global bias-correction scheme used in IMERG. These factors should be considered when extending the present findings to other basins or temporal scales.

Author Contributions: The contributions of each author are as follows: F.F.B.: Conceptualization, Methodology, Validation, Formal Analysis, Investigation, Data Curation, Writing—Original Draft, Visualization; D.T.R.: Conceptualization, Methodology, Supervision, Writing—Review and Editing; C.M.S.e.S.: Conceptualization, Methodology, Supervision, Writing—Review and Editing; L.d.M.B.A.: Writing—Review and Editing; P.R.M.: Writing—Review and Editing; M.P.: Writing—Review and Editing; M.J.C.: Writing—Review and Editing. All authors have read and agreed to the published version of the manuscript.

Funding: This research was funded in part by the Federal Institute of Espírito Santo (IFES), through the PRODIF program, and in part by the Federal University of Rio Grande do Norte (UFRN), through CAPES–Brazilian Federal Agency for Support and Evaluation of Graduate Education (Finance Code 001). M.P. and M.J.C. are funded by national funds through FCT–Fundação para a Ciência e Tecnologia, I.P., in the framework of the UID/06107/2023–Center for Sci-Tech Research in Earth

System and Energy (CREATE). The Article Processing Charge (APC) was also funded by IFES (PRODIF) and UFRN (CAPES—Finance Code 001).

Data Availability Statement: Data will be made available on request.

Acknowledgments: The authors acknowledge the institutional support provided by the Federal Institute of Espírito Santo (IFES) and the Federal University of Rio Grande do Norte (UFRN), particularly through research infrastructure, academic collaboration, and graduate training support. We are thankful to the National Council for Scientific and Technological Development (CNPq) for the research productivity grant of the second author (Process no 311283/2025-0) and third author (Process no 310781/2020-5).

Conflicts of Interest: The authors declare that they have no known competing financial interests or personal relationships that could have appeared to influence the work reported in this paper.

References

1. Lee, H.; Calvin, K.; Dasgupta, D.; Krinner, G.; Mukherji, A.; Thorne, P.; Trisos, C.; Romero, J.; Aldunce, P.; Barret, K.; et al. *IPCC, 2023: Climate Change 2023: Synthesis Report, Summary for Policymakers. Contribution of Working Groups I, II and III to the Sixth Assessment Report of the Intergovernmental Panel on Climate Change*; Core Writing Team, Lee, H., Romero, J., Eds.; IPCC: Geneva, Switzerland, 2023. [CrossRef]
2. Rudorff, C.; Sparrow, S.; Guedes, M.R.; Tett, S.F.; Brêda, J.P.L.; Cunningham, C.; Ribeiro, F.N.; Palharini, R.S.; Lott, F.C. Event attribution of Parnaíba River floods in Northeastern Brazil. *Clim. Resil. Sustain.* **2022**, *1*, e16. [CrossRef]
3. Gadelha, A.N.; Coelho, V.H.R.; Xavier, A.C.; Barbosa, L.R.; Melo, D.C.; Xuan, Y.; Huffman, G.J.; Petersen, W.A.; Almeida, C.D.N. Grid box-level evaluation of IMERG over Brazil at various space and time scales. *Atmos. Res.* **2019**, *218*, 231–244. [CrossRef]
4. Hosseini-Moghari, S.-M.; Tang, Q. Validation of GPM IMERG V05 and V06 Precipitation Products over Iran. *J. Hydrometeorol.* **2020**, *21*, 1011–1037. [CrossRef]
5. Huffman, G.J.; Bolvin, D.T.; Joyce, R.; Kelley, O.A.; Nelkin, E.J.; Portier, A.; Stocker, E.F.; Tan, J.; Watters, D.C.; West, B.J. *IMERG V07 Release Notes*; Goddard Space Flight Center: Greenbelt, MD, USA, 2023. Available online: https://gpm.nasa.gov/data/news (accessed on 17 June 2025).
6. Guo, H.; Tian, Y.; Li, J.; Guo, C.; Meng, X.; Wang, W.; De Maeyer, P. Has IMERG_V07 Improved the Precision of Precipitation Retrieval in Mainland China Compared to IMERG_V06? *Remote Sens.* **2024**, *16*, 2671. [CrossRef]
7. Liu, Z.; Hou, H.; Zhang, L.; Hu, B. Event-Based Bias Correction of the GPM IMERG V06 Product by Random Forest Method over Mainland China. *Remote Sens.* **2022**, *14*, 3859. [CrossRef]
8. Watters, D.C.; Gatlin, P.N.; Bolvin, D.T.; Huffman, G.J.; Joyce, R.; Kirstetter, P.; Nelkin, E.J.; Ringerud, S.; Tan, J.; Wang, J.; et al. Oceanic Validation of IMERG-GMI Version 6 Precipitation Using the GPM Validation Network. *J. Hydrometeorol.* **2024**, *25*, 125–142. [CrossRef]
9. Ramadhan, R.; Marzuki, M.; Suryanto, W.; Sholihun, S.; Yusnaini, H.; Muharsyah, R. Validating IMERG data for diurnal rainfall analysis across the Indonesian maritime continent using gauge observations. *Remote Sens. Appl.* **2024**, *34*, 101186. [CrossRef]
10. Wang, Y.; Li, Z.; Gao, L.; Zhong, Y.; Peng, X. Comparison of GPM IMERG Version 06 Final Run Products and Its Latest Version 07 Precipitation Products across Scales: Similarities, Differences and Improvements. *Remote Sens.* **2023**, *15*, 5622. [CrossRef]
11. Rozante, J.R.; Rozante, G. IMERG V07B and V06B: A Comparative Study of Precipitation Estimates Across South America with a Detailed Evaluation of Brazilian Rainfall Patterns. *Remote Sens.* **2024**, *16*, 4722. [CrossRef]
12. Shimizu, M.H.; Anochi, J.A.; Kayano, M.T. Precipitation patterns over northern Brazil basins: Climatology, trends, and associated mechanisms. *Theor. Appl. Climatol.* **2022**, *147*, 767–783. [CrossRef]
13. ANA. *Conjuntura dos Recursos Hídricos: Informe 2016*; Agência Nacional de Águas—Brasília (ANA): Brasília, Brazil, 2016.
14. Souza, C.D.d.e.; Matos, A.J.S. *Operação do Sistema de Alerta Hidrológico da Bacia do Rio Parnaiba—2022*; Serviço Geológico do Brasil—CPRM: Teresina, Brazil, 2022. Available online: https://www.cprm.gov.br/sace/parnaiba (accessed on 8 September 2025).
15. Alvares, C.A.; Stape, J.L.; Sentelhas, P.C.; Gonçalves, J.D.M.; Sparovek, G. Köppen's climate classification map for Brazil. *Meteorol. Z.* **2013**, *22*, 711–728. [CrossRef]
16. Reis, L.C.D.; Silva, C.M.S.E.; Bezerra, B.G.; Spyrides, M.H.C. Caracterização da variabilidade da precipitação no MATOPIBA, região produtora de soja (Vol. 13, Número 04). Revista Brasileira de Geografia Física. 2020. Available online: https://periodicos.ufpe.br/revistas/rbgfe (accessed on 1 September 2025).
17. de Abreu, L.P.; Mutti, P.R.; Lima, K.C. Variabilidade espacial e temporal da precipitação na bacia hidrográfica do Rio Parnaíba, Nordeste do Brasil. *Rev. Bras. De Meio Ambiente* **2019**, *7*, 082–097. [CrossRef]

18. Motta, E.D.O.; Gonçalves, N.E.W. *Plano Nascente Parnaíba: Plano de Preservação e Recuperação de Nascentes da Bacia do Rio Parnaíba*; Companhia de Desenvolvimento dos Vales do São Francisco e do Parnaíba (Codevasf)/Editora IABS: Brasília, Brazil, 2016; Available online: http://jbb.ibict.br//handle/1/689 (accessed on 8 September 2025).
19. Macedo, M.J.H.; Santos, F.A.C.; de Sousa, F.D.A.S. Geoprocessamento aplicado as características físicas e biofísicas da Bacia Hidrográfica do Rio Parnaíba. *Revista de Geografia* **2017**, *34*. [CrossRef]
20. Nascimento, J.R.S.D.; Marcuzzo, F.F.N.; Pinto, E.J.A. Mapas Da Distribuição Anual e Mensal De Chuva e Pluviograma Da Bacia Hidrográfica do Rio Parnaíba. 2020. Available online: http://rigeo.cprm.gov.br/jspui/handle/doc/18492 (accessed on 21 May 2025).
21. Xavier, A.C.; Scanlon, B.R.; King, C.W.; Alves, A.I. New improved Brazilian daily weather gridded data (1961–2020). *Int. J. Climatol.* **2022**, *42*, 8390–8404. [CrossRef]
22. Xavier, A.C.; King, C.W.; Scanlon, B.R. Daily gridded meteorological variables in Brazil (1980–2013). *Int. J. Climatol.* **2016**, *36*, 2644–2659. [CrossRef]
23. Huffman, G.J.; Bolvin, D.T.; Braithwaite, D.; Hsu, K.L.; Joyce, R.J.; Kidd, C.; Nelkin, E.J.; Sorooshian, S.; Stocker, E.F.; Tan, J.; et al. Integrated Multi-satellite Retrievals for the Global Precipitation Measurement (GPM) Mission (IMERG). In *Satellite Precipitation Measurement*; Springer International Publishing: Cham, Switzerland, 2020; pp. 343–353. [CrossRef]
24. Campos, J.A.; da Silva, D.D.; Pires, G.F.; Amorim, R.S.S.; de Menezes Filho, F.C.M.; de Melo Ribeiro, C.B.; Lorentz, J.F.; Aires, U.R.V. Modeling Environmental Vulnerability for 2050 Considering Different Scenarios in the Doce River Basin, Brazil. *Water* **2024**, *16*, 1459. [CrossRef]
25. de Andrade, J.M.; Neto, A.R.; Bezerra, U.A.; Moraes, A.C.C.; Montenegro, S.M.G.L. A comprehensive assessment of precipitation products: Temporal and spatial analyses over terrestrial biomes in Northeastern Brazil. *Remote Sens. Appl.* **2022**, *28*, 100842. [CrossRef]
26. Bender, F.D.; Sentelhas, P.C. Solar Radiation Models and Gridded Databases to Fill Gaps in Weather Series and to Project Climate Change in Brazil. *Adv. Meteorol.* **2018**, *2018*, 6204382. [CrossRef]
27. Melo, D.D.C.; Xavier, A.C.; Bianchi, T.; Oliveira, P.T.; Scanlon, B.R.; Lucas, M.C.; Wendland, E. Performance evaluation of rainfall estimates by TRMM Multi—Satellite Precipitation Analysis 3B42V6 and V7 over Brazil. *J. Geophys. Res. Atmos.* **2015**, *120*, 9426–9436. [CrossRef]
28. Ward, J.H. Hierarchical Grouping to Optimize an Objective Function. *J. Am. Stat. Assoc.* **1963**, *58*, 236–244. [CrossRef]
29. Rodrigues, D.T.; Gonçalves, W.A.; Spyrides, M.H.C.; Silva, C.M.S.E. Spatial and temporal assessment of the extreme and daily precipitation of the Tropical Rainfall Measuring Mission satellite in Northeast Brazil. *Int. J. Remote Sens.* **2020**, *41*, 549–572. [CrossRef]
30. Silva, M.E.S.; da Rocha, R.P.; Pereira, G.; Rocha, A.M.; Mendes, D.; da Silva, C.B. The combined influences of Amazon deforestation and Pacific Decadal Oscillation on the South America climate variability. *Int. J. Climatol.* **2023**, *43*, 2127–2149. [CrossRef]
31. Santos e Silva, C.M.; Rodrigues, D.T.; Medeiros, F.; Valentim, A.M.; de Araújo, P.A.A.; da Silva Pinto, J.; Mutti, P.R.; Mendes, K.R.; Bezerra, B.G.; de Oliveira, C.P.; et al. Diurnal cycle of precipitation in Brazil. *Theor. Appl. Climatol.* **2024**, *155*, 7811–7826. [CrossRef]
32. Everitt, B.S.; Landau, S.; Leese, M.; Stahl, D. *Cluster Analysis*, 5th ed.; John Wiley & Sons Ltd.: West Sussex, UK, 2011. [CrossRef]
33. Romesburg, H.C. *Cluster Analysis for Researchers*; Reprint of 1984 edit; Lulu Press: Morrisville, NC, USA, 2004.
34. Wilks, D.S. Statistical Methods in the Atmopspheric Sciencies. In *International Geophycs Series*; Academic press: Cambridge, MA, USA, 2011; p. 649.
35. Morais, R.C.D.S.; De Abreu, L.P. Análise Espacial Da Variabilidade De Precipitação Na Bacia Hidrográfica Do Rio Parnaíba, Nordeste De Brasil Spatial Analysis of Precipitation Variability in Parnaíba River Watershed, Northeast of Brazil. *Rev. Acad. Ciências Piauí* **2021**, *2*, 3–18. [CrossRef]
36. Zhang, M.; de Leon, C.; Migliaccio, K. Evaluation and comparison of interpolated gauge rainfall data and gridded rainfall data in Florida, USA. *Hydrol. Sci. J.* **2018**, *63*, 561–582. [CrossRef]
37. Zhao, K.; Zhong, S. Evaluation and Error Analysis of Multi-Source Precipitation Datasets during Summer over the Tibetan Plateau. *Atmosphere* **2024**, *15*, 165. [CrossRef]
38. Polasky, A.; Sapkota, V.; Forest, C.E.; Fuentes, J.D. Discrepancies in precipitation trends between observational and reanalysis datasets in the Amazon Basin. *Sci. Rep.* **2025**, *15*, 7268. [CrossRef]
39. Rasera, J.B.; Silva, R.F.D.; Piedade, S.; Mourão Filho, F.D.A.A.; Delbem, A.C.B.; Saraiva, A.M.; Sentelhas, P.C.; Marques, P.A.A. Do Gridded Weather Datasets Provide High-Quality Data for Agroclimatic Research in Citrus Production in Brazil? *AgriEngineering* **2023**, *5*, 924–940. [CrossRef]
40. Batista, F.F.; Rodrigues, D.T.; Santos e Silva, C.M. Analysis of climatic extremes in the Parnaíba River Basin, Northeast Brazil, using GPM IMERG-V6 products. *Weather. Clim. Extrem.* **2024**, *43*, 100646. [CrossRef]
41. dos Santos, A.L.M.; Gonçalves, W.A.; Rodrigues, D.T.; Andrade, L.d.M.B.; e Silva, C.M.S. Evaluation of extreme precipitation indices in Brazil's semiarid region from satellite data. *Atmosphere* **2022**, *13*, 1598. [CrossRef]

42. Xu, F.; Zhou, Y.; Zhao, L. Spatial and temporal variability in extreme precipitation in the Pearl River Basin, China from 1960 to 2018. *Int. J. Climatol.* **2022**, *42*, 797–816. [CrossRef]
43. Tinôco, I.C.M.; Bezerra, B.G.; Lucio, P.S.; Barbosa, L.M. Characterization of Rainfall Patterns in the Semiarid Brazil. *Anuário Inst. Geociências—UFRJ* **2018**, *41*, 397–409. [CrossRef]
44. Guedes, R.D.S.; Lima, F.D.; Amanajás, J.C.; Braga, C.C. Análise Em Componentes Principais Da Precipitação Pluvial No Estado Do Piauí e Agrupamento Pelo Método De Ward. *Rev. Geogr.* **2010**, *27*, 218–233.
45. Lyu, X.; Li, Z.; Li, X. Evaluation of Gpm Imerg Satellite Precipitation Products in Event-Based Flood Modeling over the Sunshui River Basin in Southwestern China. *Remote Sens.* **2024**, *16*, 2333. [CrossRef]
46. Couto, F.T.; Ducrocq, V.; Salgado, R.; Costa, M.J. Numerical simulations of significant orographic precipitation in Madeira island. *Atmos Res.* **2016**, *169*, 102–112. [CrossRef]
47. Couto, F.T.; Ducrocq, V.; Salgado, R.; Costa, M.J. Understanding significant precipitation in Madeira island using high—Resolution numerical simulations of real cases. *Q. J. R. Meteorol. Soc.* **2017**, *143*, 251–264. [CrossRef]
48. Costa, M.J.; Salgado, R.; Santos, D.; Levizzani, V.; Bortoli, D.; Silva, A.M.; Pinto, P. Modelling of orographic precipitation over Iberia: A springtime case study. *Adv. Geosci.* **2010**, *25*, 103–110. [CrossRef]